Defence Science Journal, Vol. 67, No. 2, March 2017, pp. 224-229, DOI : 10.14429/dsj.67.9850

FDTD Modelling of 1D Photonic Crystal for Thermal Masking Application with CPML Absorbing Boundary Condition

M. Ashok Kumar, N.P. Anusha, and Alok Sharan*

Department of Physics, Pondicherry University, Puducherry - 605 014, India
**E-mail: aloksharan@gmail.com*

ABSTRACT

Periodic structures of double positive and double negative metamaterial of thickness of λ/4 is designed to stop long-wave infrared and mid-wave infrared frequencies for masking from infrared detection devices. Band-gaps are obtained by calculating reflection and transmission coefficients at probe point close to the front and back faces of the periodic structure. 1D- finite difference time domain method is implemented in Matlab to study the electromagnetic wave propagation which is incident normal to a periodic stack of double positive and double negative metamaterial of having refractive indices of 9 and -6 respectively, at centre wavelength. Drude model is adapted to model double negative medium. Band-gap obtained are compared with the conventional photonic crystal by replacing the double negative medium with a double positive medium with the magnitude of refractive index same as that of double negative medium. Band-gap obtained confirms the presence of Zero-ñ band-gap in DPS-DNG photonic crystal which is wider than the reflection band in conventional photonic crystal; nearly twice in mid-wave infrared region and five times in long-wave infrared region. A novel and highly efficient convolutional perfectly matched layer absorbing boundary condition is used to terminate the infinite computational finite difference time domain lattices.

Keywords: Photonic crystal; Finite difference time domain; Zero-ñ band gap; Double positive and double negative; Thermal imaging; Convolutional perfectly matched layer

NOMENCLATURE

Γ	Dissipation factor in Drude model
J_x	Electric current density
K_y	Magnetic current density
ω_{pe}	Electric plasma frequency
ω_{pm}	Magnetic plasma frequency
k_0	Wave vector correspond to mid band frequency
Δ_t	Time step in FDTD
Δ_z	Grid size in FDTD
λ_0	Wave length corresponds to mid band frequency
c	Speed of light in vacuum
ψ_{hyz}	Convolution term in CPML
α_z, b_z, k_z, a_z	Convolutional parameters in CPML
σ_z	Conductivity profile in CPML
W	Energy density
ñ	Volume averaged zero refractive index

1. INTRODUCTION

Thermal emission in infrared region from an object gives the information about size and nature of target in the battle field via thermal imaging devices. Thermal emission of tanks and soldiers in the battle field can be clearly identified by thermal imaging devices operating in long-wave infrared region (LWIR) even in arenaceous environment. Heat seeking missiles which are guided by infrared imaging devices use mid-wave infrared (MWIR) to lock the moving target[1-4]. Infrared camouflage is a counter-measure to avoid opponent attack. Intense research in the defence establishments is focussed on the thermal masking of an object from heat seeking and night vision sensors.

Thermal masking is possible by utilising photonic crystal based meta-materials and nano-materials. Numerical investigation and laboratory tests of thermal absorbers for camouflaging target in MWIR and LWIR regions show that absorbance does not cover entire infrared region[4]. Meta-material based perfect absorbers fabricated from metal-dielectric disks having multiband absorption in MWIR and LWIR[5,6] regions can be used for thermal masking application. But their absorbance is high only at particular wavelengths. There may be leakage of other wavelengths in MWIR and LWIR regions. Another example of perfect absorbers of mid-wave infrared wave is multiplexed metal structures, which absorbs in a narrow window within MWIR region[7]. To overcome the leakage, an additional coating can be done for achieving zero transmission in the wide-band of MWIR and LWIR frequencies. The frequencies which leaks will get reflected back within the material and thereby camouflaging the object from heat seeking devices.

Apart from thermal camouflage, the wide-band reflection in infrared region can be used as a counter measure for missile jamming and shielding the missiles from high energy infrared lasers operating in MWIR and LWIR region. The wide-tunable mid-infrared quantum cascade lasers is used in airborne

Received : 10 March 2015, Revised : 22 October 2016
Accepted : 06 February 2017, Online published : 11 March 2017

defence systems is interfaced with missile warning systems in the aircraft. It is used for damaging the infrared imaging sensor in the heat seeking missiles[8,9]. This can be overcome by temporarily blocking mid-wave infrared laser with wide-band reflection coating. The coating may reflect the high energy beam from the infrared laser directed towards the incoming missile, and it act as a shield for the missile.

In this report thermal masking over wide range of MWIR and LWIR frequencies using photonic crystal made of Double positive (DPS) and Double negative (DNG) materials is propose. Conventional photonic crystal consists of two materials having different dielectric constants arranged in periodic order and it can forbid particular range of frequencies[10,11]. The band-gap in this conventional photonic crystal is formed due to the Bragg scattering of fields from the periodic structure. Instead of two dielectric materials if one of the dielectric materials is replaced with a DNG medium, an unconventional photonic crystal is obtained. If volume averaged refractive index of this DPS-DNG photonic crystal is zero, it shows high reflecting property for specific range of frequencies. The band-gap formed due to the volume averaged zero refractive index in these kind of structure is termed as zero-ñ gap[13,14]. Both Bragg gap and zero-ñ gap can be present in a DPS-DNG photonic crystal. Zero-ñ gap is invariant of length scale changes[15] and hence it can be differentiated from Bragg gap, which varies with the thickness of unit cell. This unconventional photonic crystal has a broader reflection range over the conventional photonic crystal[12-17]. Width of zero-ñ gap in this unconventional photonic crystal can be controlled by properly choosing the appropriate separation between electric and magnetic plasma frequencies. Volume averaged zero refractive index in the proposed periodic structure, with wider stop-band for long-wave and mid-wave infrared regions has been achieved. These results are also compared with conventional photonic crystal with identical simulation parameters.

2. FDTD MODELLING OF DPS-DNG AND DIELECTRIC PERIODIC STRUCTURE

Veselago[18] proposed a medium with negative values for dielectric permittivity and magnetic permeability simultaneously. For a dispersive medium where the permittivity and permeability are functions of applied frequency, the response of the medium depends on the history of the applied field. The response of the medium follows the applied field below the resonant frequency and is out of phase for the frequency above the resonance. If the resonant frequency region is made ultra-narrow, it is possible to achieve negative values for real part of effective permittivity and permeability[19,20].

Maxwell equation for a plane monochromatic harmonic wave is represented as

$$\bar{k}\times\bar{H} = -\omega\varepsilon_0\varepsilon\bar{E}$$
$$\bar{k}\times\bar{E} = -\omega\mu_0\mu\bar{H} \quad (1)$$

Electric field $\bar{E}$, magnetic field $\bar{H}$ and propagation vector $\bar{k}$ form left hand orthogonal system at close to resonance frequency for material having real part of electric permittivity and magnetic permeability to be negative. Medium possessing these values are left handed medium (LHM) or DNG medium[19,21]. In DPS medium these vectors form a right hand system. The Poynting vector $\bar{S}$, electric field $\bar{E}$ and the magnetic field $\bar{H}$ form a right hand orthogonal system both in the DPS and DNG medium.

The equation of energy density for a DNG medium is

$$W = \frac{\partial(\varepsilon\omega)}{\partial\omega}E^2 + \frac{\partial(\mu\omega)}{\partial\omega}H^2 \quad (2)$$

The necessary condition for energy density with simultaneous negative permittivity and permeability[18] is

$$\frac{\partial(\varepsilon\omega)}{\partial\omega} > 0 \; and \; \frac{\partial(\mu\omega)}{\partial\omega} > 0 \quad (3)$$

This doesn't require ε and μ to be simultaneously negative. But the DNG medium should necessarily be dispersive. Hence Drude dispersive model is used to simulate the DNG medium in this article.

The Maxwell's equations for a DNG medium can be written as

$$\partial_t E_x = \frac{1}{\varepsilon_0}\left(-\partial_z H_y - J_x\right)$$
$$\partial_t H_y = -\frac{1}{\mu_0}\left(\partial_z E_x + K_y\right) \quad (4)$$

where J_x is electric current density and K_y is magnetic current density and are written using Drude model[21,22] as

$$\partial_t J_x + \Gamma J_x = \varepsilon_0\omega_{pe}^2 E_x$$
$$\partial_t K_y + \Gamma\ K_y = \mu_0\omega_{pm}^2 H_y \quad (5)$$

where ω_{pe} and ω_{pm} are plasma frequencies of the material and Γ is the dissipation factor. Γ = 0 is used in this report.

Maxwell's equations for a DPS medium is given by

$$\partial_t E_x = -\frac{1}{\varepsilon_0}\left(\partial_z H_y\right)$$
$$\partial_t H_y = -\frac{1}{\mu_0}\left(\partial_z E_x\right) \quad (6)$$

Standard Yee algorithm[23] is used in this paper to discretise electric and magnetic fields in leap frog arrangement in finite difference time domain (FDTD) lattice space.

FDTD method is a numerical technique to solve partial differential equation which describes the wave motion. It uses set of finite difference equations to solve time- dependent Maxwell's equation with central difference approximation for numerical derivatives in space and time. FDTD method is used to solve the coupled Maxwell's equation.

Yee algorithm can be summarised as:

- Differential form of Ampere's law and Faraday's law are replaced with finite difference equations using central difference formula.
- The components of electric field $\bar{E}$ and magnetic field $\bar{H}$ are interleaved in space and time which is referred as leapfrog arrangement. The fields are calculated from discretised finite difference updated equations. The unknown value of electric field is calculated using known value of electric field and past values of magnetic field, which is stored in the memory. Similarly future magnetic field is calculated from the known value of magnetic field and past values of electric field which is stored in computer memory. This process is repeated until desired time step is attained.

The electric field is located at the cell edges for integral time step and the magnetic field is located at the cell center for half integral time step. Electric and magnetic current densities are located at the cell centers[21,22]. Total field/Scattered field (TF/SF) formalism is used to introduce the source in the FDTD lattice. Total field region contains incident field, scattering object (periodic structure in this case) and scattered field whereas scattered field region contains only the field scattered by the object[23].

Convolutional perfectly matched layer (CPML) absorbing boundary condition is used to terminate FDTD lattice. CPML is completely independent of host medium and hence is used to model different kinds of materials which are dispersive and anisotropic. Also, it effectively reduces the late time reflection from the boundary. The CPML boundary condition equation which is used to terminate 1D-FDTD[23,24] grid, is given as

$$\mu_r\mu_0\frac{H_y^{n+1}-H_y^n}{\Delta t}+\sigma\frac{H_y^{n+1}-H_y^n}{2}=-\frac{(E_x^{n+1/2}-E_x^{n+1/2})}{k_z\Delta_z}+\psi_{hyz}^{n+1/2} \quad (7)$$

$$\psi_{hyz}^{n+1/2}=b_z\psi_{hyz}^{n-1/2}+a_z\frac{(E_x^{n+1/2}-E_x^{n+1/2})}{\Delta_z} \quad (8)$$

$$b_z=\exp-\left(\left(\frac{\sigma_z}{k_z}\right)+\alpha_z\right)\left(\frac{\Delta t}{\varepsilon_0}\right)$$

$$a_z=\frac{\sigma_z}{\left(\sigma_z k_z+k_z^2\alpha_z\right)}\left(b_z-1\right)$$

2.1 Simulation Parameters

Periodic structure with alternate DPS and DNG layers are constructed with 15 periods. Each layer in the period has a thickness of $\lambda_0/4$ so chosen to obtain stop band in the region of LWIR (8 µm - 15 µm) and MWIR (3 µm - 5 µm). The reference wavelength λ_0 is chosen as 12 µm and 4µm for LWIR and MWIR region respectively. Time differentiated Gaussian pulse of band width 110THz is incident at normal to the periodic structure. Ten cells at the left side and twelve cells at the right side are set as CPML region to terminate FDTD lattices. The conductivity and convolutional parameters in the CPML region is optimised to get minimum reflection from the terminating boundary[24]. The TF/SF boundary begins five cells away from the left boundary. Reflected field is recorded one cell before the TF/SF boundary and transmitted field is recorded one cell after the exit of the periodic structure. The reflection and transmission coefficients are calculated by taking the FFT of reflected and transmitted fields. Refractive indices for DPS-DNG periodic structure are chosen to be n_1=9 and n_2= -6 and for dielectric periodic structure refractive indices are chosen as n_1=9 and n_2=6. The thicknesses are calculated using the formula[25].

$$n_1d_1=n_2d_2=\lambda_0/4=\pi c/2\omega_0 \quad (9)$$

where d_1 and d_2 are the thicknesses of the layer in periodic structure.

3. RESULTS AND DISCUSSION

The frequency dependence of electric permittivity and magnetic permeability are given by

$$\varepsilon(\omega)=\varepsilon_0[1-\frac{\omega_{pe}^2}{\omega(\omega+i\Gamma)}]$$

$$\mu(\omega)=\mu_0[1-\frac{\omega_{pm}^2}{\omega(\omega+i\Gamma)}] \quad (10)$$

where ω is the frequency of incident field.

The real part of these frequency dependent permittivity and permeability, in LWIR frequency range, are plotted in Fig. 1; for plasma frequencies of ω_{pe} = 496.73 THz, ω_{pm} =351.24 THz and Γ=0. In region III of Fig. 1 both permittivity and permeability are positive which the case of conventional DPS materials is. In region II permittivity is negative and permeability is positive and the wave propagation is forbidden in this range of frequency, since the wave vector becomes imaginary. In region I both permeability and permittivity are negative for the above mentioned frequencies. In this frequency range, materials behave as DNG medium. The values of permeability and permittivity lying in region I is considered in this study.

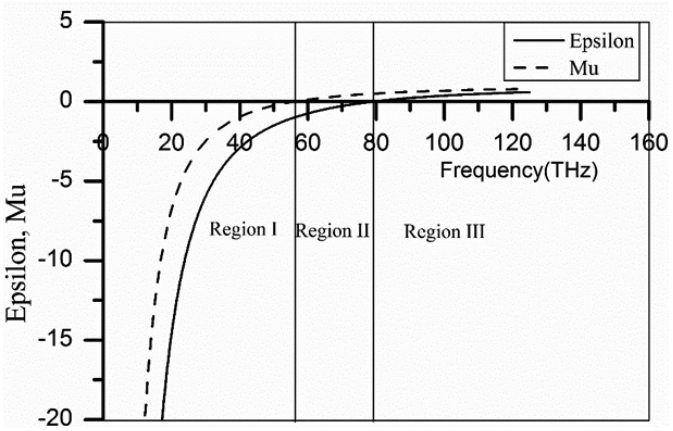

Figure 1. Frequency dependent permittivity and permeability.

Figure 2 shows the Fourier transform of reflected and transmitted field from conventional photonic crystal. It indicates the region where reflection is maximum and transmission is zero for small range of frequencies in LWIR region. Reflection and transmission coefficient are calculated and the band-gap is obtained in the region of LWIR from 22.88 THz to 26.82 THz as shown in Fig. 2(c). The total computational domain consisting of 2177 grids is discretised with FDTD lattice dimension of Δz =5.802 nm and lattice constant of a= 833.3 nm.

For the same photonic crystal, the reflection and the transmission coefficients for MWIR region is shown in Fig.3. We obtain the band-gap from 66.2THz to 84.02 THz. The lattice dimension used is Δz=5.802nm and lattice constant is a= 277.7 nm.

For both the cases, width of the band-gap is very small, 3.94 THz and 17.82 THz for LWIR and MWIR frequencies, respectively. For increasing the band-width of band-gap, unconventional DPS-DNG photonic crystal structure is used and the results are as follows.

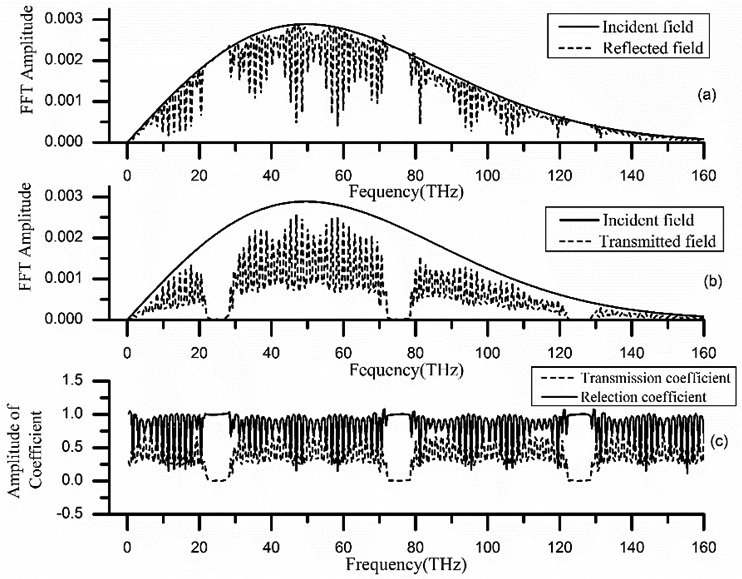

Figure 2. (a) FFT of reflected wave, (b) FFT of transmitted wave, and (c) Reflection and transmission coefficient for conventional photonic crystal in LWIR region.

Fourier transformed amplitudes of reflected and transmitted field for unconventional photonic crystal containing alternate DPS and DNG media are shown in Fig. 4. The plots show wider band-width in LWIR region than conventional photonic crystal as shown in Fig. 2.

Figure 5(a) shows spatial averaged refractive index (ñ) plot for one unit cell of DPS-DNG photonic crystal in the LWIR region. The refractive index is calculated numerically by using the formula[21].

$$n_{FDTD} = \frac{1}{ik_0\left(z_2 - z_1\right)} \ln\left[\frac{E_x\left(z_2, \omega\right)}{E_x\left(z_1, \omega\right)}\right] \qquad (11)$$

where $E_x(z_2, \omega)$ and $E_x(z_1, \omega)$ are the electric fields recorded at z_1 and z_2..

The value of n_{FDTD} is close to zero for certain range of frequencies. Small deviation from near zero value is observed in some region. This is due to the numerical calculation of refractive index using the calculated electric field in the medium which propagates through discretised FDTD lattice .This field interfere with electric field reflected from each slab in the photonic crystal, and as a result there is small fluctuations in the obtained numerical refractive index.

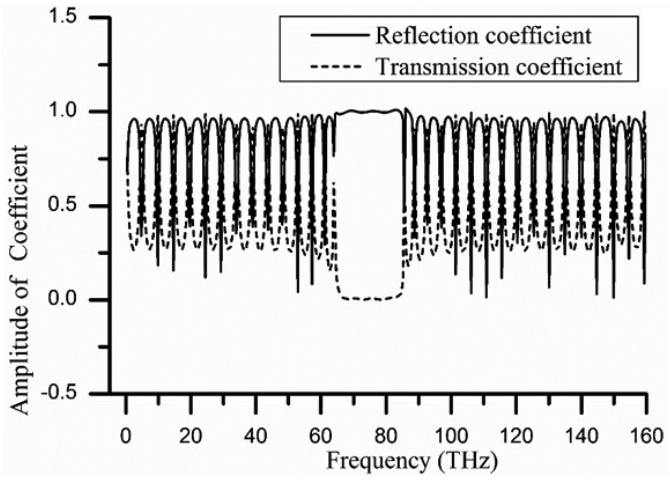

Figure 3. Reflection and transmission coefficient for conventional photonic crystal in MWIR region.

Figure 5 (b) is a plot of reflection and transmission coefficient of the field in the LWIR region. . The band-gap from 17.75 THz to 36.29 THz in the plot corresponds to zero ñ. This region is called zero ñ gap regions. Here the band gap is nearly five times wider than that of conventional photonic crystal as seen in Fig. 2(c). This wider band- width is due to the high reflecting property of volume averaged refractive index ñ = -3.60E-4 which is close to zero. This value is consistent with ñ= 2.324E-4 is given[14]. Two more band-gaps from 71.79 THz to 98.61 THz and from 108.9 THz to 148.87 THz are observed in the plot. The thickness of periodic structure layer is varied and the band-gaps are tested. It is seen that when the thickness varies the width and position of the band-gaps does not change, which confirms that the gaps are due to zero-ñ. The results are as shown in Table 1.

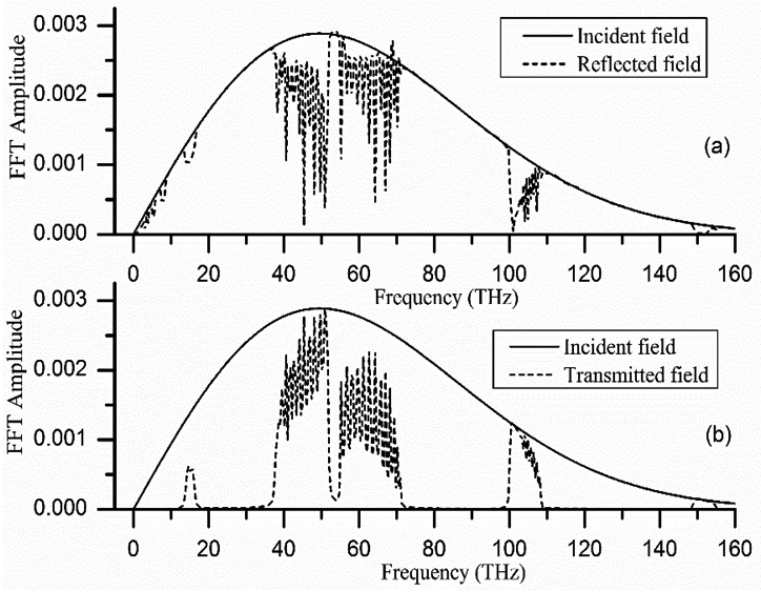

Figure 4. (a) FFT of reflected wave and (b) FFT of transmitted wave, for DPS-DNG photonic crystal in LWIR region.

Table 1. Bandgap values for different thickness of DPS and DNG photonic crystal in LWIR region

Thickness of DPS (nm)	Thickness of DNG (nm)	Band gaps (THz)		
		First	Second	Third
333.3	500	17.75 - 36.29	71.79 -98.61	108.9-148.87
339.3	506	17.75 - 36.29	71.79 -97.43	108.9 -148.7

Figure 6 (a) is the plot of numerically calculated refractive index of DPS-DNG structure in MWIR region and Fig. 6(b) is plot of reflection and transmission coefficient for MWIR region. Fig. 6(b) gives a zero-ñ gap from 59.9 THz to 92.3 THz which is more than that of conventional photonic crystal in MWIR region as seen in Fig. 3(c). In the figure two more

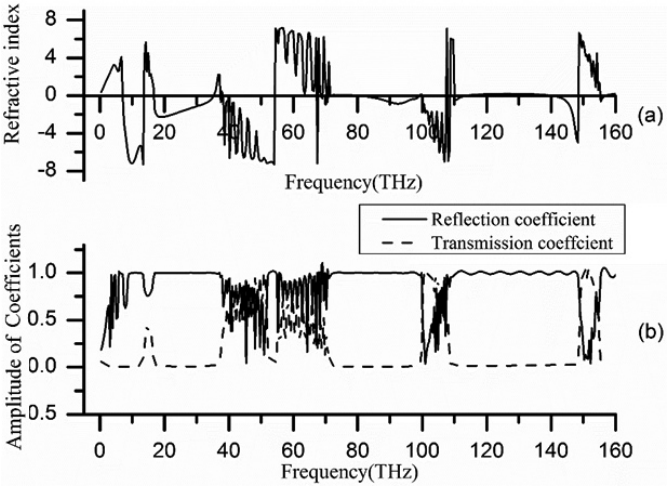

Figure 5. (a) Refractive index in DPS-DNG photonic crystal using FDTD for LWIR region and (b) Reflection and transmission coefficient for DPS-DNG photonic crystal in LWIR region.

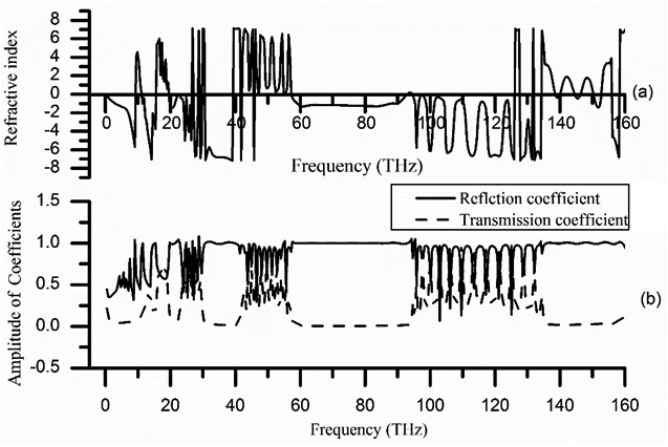

Figure 6. (a) Refractive index in DPS-DNG photonic crystal using FDTD for MWIR region and (b) Reflection and transmission coefficient for DPS-DNG photonic crystal in MWIR region.

band-gaps are noticed from 30.77 THz to 40.6 THz and from 134.9 THz to 157.7 THz as shown in Table 2. Here when the thickness of periodic structure changes, the width of third band gap shifts from 134.1 THz to 150.3 THz which shows that this band-gap alone is due to Bragg scattering.

Table 2. Bandgap values for different thickness of DPS and DNG photonic crystal in MWIR region

Thickness of DPS (nm)	Thickness of DNG (nm)	Band gaps(THz)		
		First	Second	Third
111.11	166.67	30.77 - 40.6	59.9- 92.3	134.9 - 157.7
117.11	172.67	30.77- 40.6	59.9 - 92.3	134.1 - 150.3

4. CONCLUSIONS

In this study, electromagnetic wave propagation in conventional dielectric photonic crystal and unconventional DPS-DNG photonic crystal are studied using FDTD code developed in-house. The band-gaps formed in both type of photonic crystal in LWIR and MWIR frequencies are studied. With proper choice of electric and magnetic plasma frequencies for DPS-DNG photonic crystal, near zero value for volume averaged refractive index, ñ is achieved. This ñ gives a zero-ñ band-gap for certain range of frequencies. This zero-ñ gap is compared with the Bragg gap formed in dielectric photonic crystal and it is observed that zero-ñ gap is wider than Bragg gap. The position and the width of zero-ñ gap are examined by changing the thickness of unit cell in DPS-DNG photonic crystal. It is shown that unlike Bragg gap, position and width of zero-ñ gap do not change with thickness of the unit cell. For DPS-DNG photonic crystal optimised in the MWIR frequency, both zero-ñ gap and Bragg gap are observed. Width of this Bragg gap is found to be dependent on the thickness of unit cell.

REFERENCES

1. Albertoni, Alessandro. Thermal scene analysis via finite element model and finite difference time domain numerical solution of the electromagnetic wave propagation in the short wave and long wave infrared band. *In* Proceedings of SPIE Vol. 7481 748106, 2004. doi: 10.1117/12.830407.
2. Albertoni, Alessandro. Long wave infrared metamaterials and nano-materials design, simulation and laboratory test for target camouflage in the defence application. *In* Proceedings of SPIE Vol. 8185 818509-1, 2011. doi:10.1117/12.898116.
3. Carlo, Kopp. Heat-seeking missile guidance Military Technology. http://indiandefence.com/threads/dr-carlo-kopps-air-to-air-missiles-review.17703/ (Accessed on 20 February 2016).
4. Albetoni, Alessandro & Perfetto, Sergio. Mid wave and long wave infrared metamaterials and nano-materials design with finite element and finite difference time domain models for target camouflage. *In* Proceedings of SPIE Vol.7834 78340U-1, 2010. doi: 10.1117/12.866443.
5. Dayal, Govind & Ramakrishna, S. Anantha. Design of multi-band metamaterial perfect absorbers with stacked metal–dielectric disks. *J. Opt.,* 2013, **15**, 055106. doi: 10.1088/2040-8978/15/5/055106
6. Singh, Govind Dayal. Metamaterials for multi-spectral infrared absorbers. Indian Institute of Technology Kanpur, India, 2014, (PhD Thesis).
7. Hendrickson, Joshua; Guo, Junpeng; Zhang, Boyang; Buchwald, Walter; & Soref, Richard. Wideband perfect light absorber at midwave infrared using multiplexed metal structures. *Optics Letters*, 2012, **37**(3) ,371-373. doi: 10.1364/OL.37.000371.
8. Takeuchi, Eric B.; Chapman, William B.; Arnone, David; Pushkarsky, Michael; Lopez, Enrique; Young, Michael; Caffey, Dave; Borgardt, Brandon; Priest, Allen; Sensibaugh, Jason; Day, Timothy. High-power, military ruggedized QCL-based laser systems. *In* Proceedings of SPIE 8373, Micro- and Nanotechnology Sensors, Systems, and Applications IV, 83732I, 2012. doi: 10.1117/12.920935

9. Espen, Lippert; Magnus, W. Haakestad & Helge, Fonnum. High-energy mid-IR laser for defense against heat-seeking missiles. *SPIE Newsroom*, 2014. doi: 10.1117/2.1201408.005572
10. Joannopoulos, J.D.; Pierre Villeneuve, R.; Shanhui, Fan. Photonic crystals: Putting a new twist on light. *Nature*, 1997, **386**, 143-149. doi: 10.1038/386143a0
11. Robertson,W.M.; Arjavalingam, G.; Meade, R.D.; Brommer, K.D.; Rappe, A.M. & Joannopoulos, J.D. Measurement of photonic band structure in a two-dimensional periodic dielectric array. *Phy. Rev. Lett.,* 1992, **68**(13), 2023-2026. doi: 10.1103/PhysRevLett.68.2023
12. Jiang, Haitao; Chen, Hong; Li, Hongqiang; Zhang, Yewen; Zi, Jian & Zhu, Shiyao. Properties of one-dimensional photonic crystals containing single-negative materials. *Physical Review E*, 2004, **69**, 066607. doi: 10.1103/PhysRevE.69.066607
13. Bloemer, Mark; Aguanno, Giuseppe D'; Scalora, Michael & Mattiucci, Nadia. Broadband omnidirectional reflection from negative index materials. *Appl. Phy. Lett.,* 2005, **87**, 261921. doi: 10.1063/1.2151251
14. Panoiu., Nicolae C.; Osgood, Richard M. ; Jr.; Zhang, Shuang & Brueck, Steven R. J. Zero band gap in photonic crystal superlattices. *J. Opt. Soc. Am. B.,* 2006, **23**(3), 506-513. doi: 10.1364/JOSAB.23.000506
15. Li, Jensen; Zhou, Lei; Chan, C.T. & Sheng, P. Photonic band gap from a stack of positive and negative index materials. *Phy. Rev. Lett.,* 2003, **90** (8), 083901-1. doi: 10.1103/PhysRevLett.90.083901
16. Thapa, Khem B.; pandey, Praveen C. & Singh, Sarika. A complete band gap in one-dimensional photonic crystal containing meta-materials. *Optoelectron. Adv. Mater. Rapid Commun.,* 2010, **4**(7), 909 - 915.
17. Kocaman, S.; Chatterjee, R.; Panoiu, N. C.; McMillan, J.F.; Yu, M.B.; Osgood, R.M.; Kwong, D.L & Wong, C.W. Observation of zeroth-order band gaps in negative-refraction photonic crystal superlattices at near-infrared frequencies. *Phy. Rev. Lett.,* 2009, **102**(20), 203905. doi: 10.1103/PhysRevLett.102.203905
18. Veselago, V. G. The electrodynamics of substances with simultaneous negative permittivity and permeability, soviet phiyscs. *Uspekhi,* 1968, **10**(4), 509-514. doi: 10.1070/PU1968v010n04ABEH003699
19. Anantha Ramakrishna ,S. Physics of negative refractive index materials, Reports on progress in physics. 2005, **68**(2), 449–521. doi:10.1088/0034-4885/68/2/R06
20. Pendry, John B. & Smith, David R. Reversing light : Negative refraction . *Physics Today*, 2004, **57**(6), 37. doi: 10.1063/1.1784272
21. Ziolkowski, Richard W. & Heyman, Ehud. Wave propagation in media having negative permittivity and permeability. *Physical Review E.*, 2001, **64**, 056625. doi: 10.1103/PhysRevE.64.056625
22. Ziolkowski, Richard W. Pulsed and CW Gaussian beam interactions with double negative metamaterial slabs. *Optics Express,* 2003 , **11**(7), 662-681. doi: 10.1364/OE.11.000662
23. Taflove, Allen & Hagness, Susan C. Computational electrodynamics finite difference time domain method . Artech House, INC. 2005, **59**,189-302.
24. Alan Roden, J. & Gedeny, Stepen D. Convolutional PML (CPML): An efficient FDTD implementation of the CFS – PML for arbitrary media. *Microwave Opt. Technol. Lett.*. 2000, **27**(5), 334-339. doi:10.1002/1098-2760(20001205)27:5<334::AID-MOP14>3.0.CO;2-A
25. Bendickson, Jon M.; Jonathan & Dowling, P. Analytic expressions for the electromagnetic mode density in finite, one-dimensional, photonic band-gap structures. *Physical Review E*, 1996, **53**(4), 4107-4120. doi: 10.1103/PhysRevE.53.4107

ACKNOWLEDGEMENT

The authors acknowledge DST-PURSE and UGC-BSR, respectively for providing financial support to carry out their research work.

CONTRIBUTORS

Mr M. Ashok Kumar received his MSc (Physics) from Bharathidasan University in 2009. Currently he is pursuing his PhD at Pondicherry University. His research area includes computational electrodynamics using FDTD method, photonic crystal, metamaterial, experimental nonlinear optics. He designed, formulated the simulations and analysed the data.

Mrs N.P. Anusha received her MSc in Physics from Pondicherry University in 2011. Currently she is doing her PhD at Pondicherry University. Her research topics include computational electrodynamics, metamaterials and photonic crystals. She contributed in the design, simulation and analysis of data.

Dr Alok Sharan, currently Assistant Professor in Department of Physics, Pondicherry University did his MSc (Physics) from University of Poona in 1990 and PhD from IIT Kanpur in 2000. He was a Visiting fellow at TIFR Mumbai and Postdoc Fellow at Materials Research Laboratory, The Pennsylvania State University PA, USA. His research interests are in experimental nonlinear optics and computational electromagnetics. He is group leader and initiated the work and the physics of the data analysed.